Int. J. Nanoelectronics and Materials **5** (2012) 149-157

# Glass forming ability and mechanical properties of $Zr_{59}Ti_5Cu_{18}Ni_8$ $Al_{10}$ bulk metallic glasses

Ali Hafs[1*] , Badis Bendjemil[1,2,3,*], Nassima Seghairi[4], Marcello Baricco[2]

[1]*LEREC, University of Badji Mokhtar, P. Box 12, 23000 Annaba, Algeria*
[2] *Università di Torino, Via P. Giuria 9, 10125 Torino, Italy*
[3] *University of 08 mai 1945,P.Box 401 , 24000 Guelma Algeria*
[4]*University of Oum El-Bouaghi, 04000 Oum El-Bouaghi, Algeria*

Received 10 Oct. 2011; Revised 5 Dec. 2011; Accepted 5 Jan. 2012

**Abstract**

Synthesis of bulk metallic glasses (BMGs) has been one of the hottest topics of research in materials science during this decade due to their very attractive physical and mechanical properties. In the present study $Zr_{59}Ti_5Cu_{18}Ni_8$ $Al_{10}$ bullk metallic glasse (BMG) were produced in a ribbon form by the single roller melt-spinning method and in rod form with diameter of 2 mm at prepared through water-cooled copper mold casting. This study is primarily devoted to compare the results obtained with the two methods of the development. Thermal properties were measured by performing DSC at at different heating rates (5, 10, 15, 20 and 25°C/mn). The microstructure and constituent phase of the alloy composite have been analyzed by using X-ray diffractometry (XRD). The mechanical properties are also studied using the compression and Vickers indentation technique, respectively and morphologies of the fractured observed by Scanning Electron Microscopy (SEM). The Energy Dispersive Spectrometer (EDS) micro-analysis is performed by measuring the energy and intensity distribution of X-ray signals generated by a focused electron beam on the specimen.

**Keywords**: Bulk metallic glasses; SEM, Fracture.
**PACS**: 64.70.pe; 68.37.Hk; 62.25.Mn.

## 1. Introduction

Metallic glasses are non-crystalline metallic alloys and thus belong to the family of vitreous solids. Metallic glasses are metastable materials obtained by rapid cooling of a melt. Their atomic structures are devoid of long-range translational periodicity like the crystalline materials, however, they possess a certain atomic arrangement in near- and next-neighbor distances (roughly below 1 nm) [1]. Metallic glasses have many qualities interesting for different fields of materials application, for example magnetism or regarding their mechanical behaviour [2]. Zr-based metallic glasses are among the most studied alloys.

In particular, Zr–Ti–Cu–Al–Ni alloys have a high glass-forming ability (GFA) corresponding to a low critical cooling rate of less than 10 $Ks^{-1}$; hence samples of several millimeters can be prepared in a glassy state [3–6]. Knowledge of the environmental stability of the different metallic glass alloys is a crucial point for their potential

*) For correspondance; E-mail : bendjemilbadis@yahoo.fr

applications, especially for those related to their mechanical properties [7]. The general mechanical properties behavior of many glassy alloys has been already reviewed [8–11].

Because of their inherent homogeneity and the lack of "weak spots", for example grain, a good resistance has the localised rupture is expected. In this paper, the critical cooling rate and non-isothermal crystallization kinetics of $Zr_{59}Ti_5Cu_{18}Ni_8\ Al_{10}$ amorphous alloy, prepared by the copper-mold casting and melt spinning method, are assessed by means of thermal analysis.

This particular alloy was selected due to its excellent glass-forming ability. The mechanical properties of the composite have been examined through compression tests and Vickers indentation technique and fracture of amorphous alloy is presented.

## 2. Experimental

An ingot of the $Zr_{59}Ti_5Cu_{18}Ni_8\ Al_{10}$ alloy (composition is given in nominal atomic percentages) was prepared by arc-melting mixtures of Zr 99.99 mass% purity, Ti 99.8 mass% purity, Cu 99.9 mass% purity , Ni 99.9 mass% purity and Al 99.9 mass% purity in an argon atmosphere purified using Ti-gettering. From the master alloy ingot, a ribbon of 5 mm width and about 30 μm thickness was prepared using a single-roller, melt spinning technique under a vacuum atmosphere. For comparison, with the bulk cylindrical sample with constant length of about 50mm and diameter ranging from 2 mm were prepared through the injection casting of the molten alloy into copper molds with cylindrical cavities. The structure of the samples was examined by X-ray diffraction (XRD) with Cu Kα ( $\lambda = 1.54056$Å) radiation. The thermal stability associated with the glass transition, supercooled liquid region and crystallization of the glassy alloys was investigated by differential scanning calorimetry (DSC) at different heating rates(5, 10, 15, 20 and 25°C/mn).Scanning electron microscopy (JEOL JSM6400F) were used for the microstructure analysis instrument equipped with an EDS accessory to check the elemental composition of the system.. Compression properties were tested by using an Instron 5581 testing machine at a strain rate of $5\times10^{-4}$ $s^{-1}$at room temperature. The hardness of the amorphous alloy of $Zr_{59}Ti_5Cu_{18}Ni_8\ Al_{10}$ was measured using a computer-controlled Duromètre Vickers Zwick/ZHV10 hardness tester. Applied load was 30N, 10N and 3N for 10 seconds. The profiles of indentation trace were analyzed by optical microscopy.

## 3. Results and discussion

Fig. 1 shows the different heating rates (5, 10, 15, 20 and 25°C/mn) DSC curves of $Zr_{59}Ti_5Cu_{18}Ni_8\ Al_{10}$ analysis was carried out for melt-spun ribbons and as-cast cylinders. In the temperature range investigated, all the curves are characterized by two exothermic peaks, revealing a multi-step crystallization path that does not depend on the way of preparation. The values of Tg, $Tx_1$, $Tx_2$ and the supercooled liquid region ($\Delta T_x$= $Tx_1$- Tg) are listed in Table 1. It is noted that with heating rate increasing the Tg, $Tx_1$ and $Tx_2$ shifted to higher temperature, suggesting that both the glass transition and crystallization are heating-rate dependence. The DSC curves indicate a small difference in glass transition temperature (*T*g), crystallization temperature (*T*x), supercooled liquid region (Δ*T*x = *T*x −*T*g) between the ribbon and rod samples, for the as cast 2 mm-diameter cylinder.

The DSC curve of the melt-spun glassy alloy ribbon is also shown for comparison. No appreciable difference in Δ*T*x and crystallization process is recognized between the melt-spun ribbon and rod, which also indicates the formation of the glassy phase.

Table 1: Summary of the glass transition temperature Tg, crystallization temperature $T_{x1}$, $T_{x2}$, and supercooled temperature region $\Delta T_x$ for the melt-spun ribbons and as-cast rod 2 mm at different heating rates.

| Heating rate (°C/mn) | $T_g$ (°C) | $T_{x1}$(°C) | $T_{x2}$(°C) | $\Delta T_x$(°C) |
|---|---|---|---|---|
| Melt spun ribbon | | | | |
| 5 | 361 | 403 | 451 | 42 |
| 10 | 362 | 405 | 451 | 43 |
| 15 | 366 | 408 | 453 | 42 |
| 20 | 368 | 410 | 455 | 42 |
| 25 | 369 | 413 | 458 | 44 |
| As cast rod of 2 mm | | | | |
| 5 | 360 | 402 | 452 | 42 |
| 10 | 361 | 403 | 454 | 42 |
| 15 | 364 | 407 | 456 | 43 |
| 20 | 367 | 409 | 458 | 42 |
| 25 | 368 | 413 | 459 | 45 |

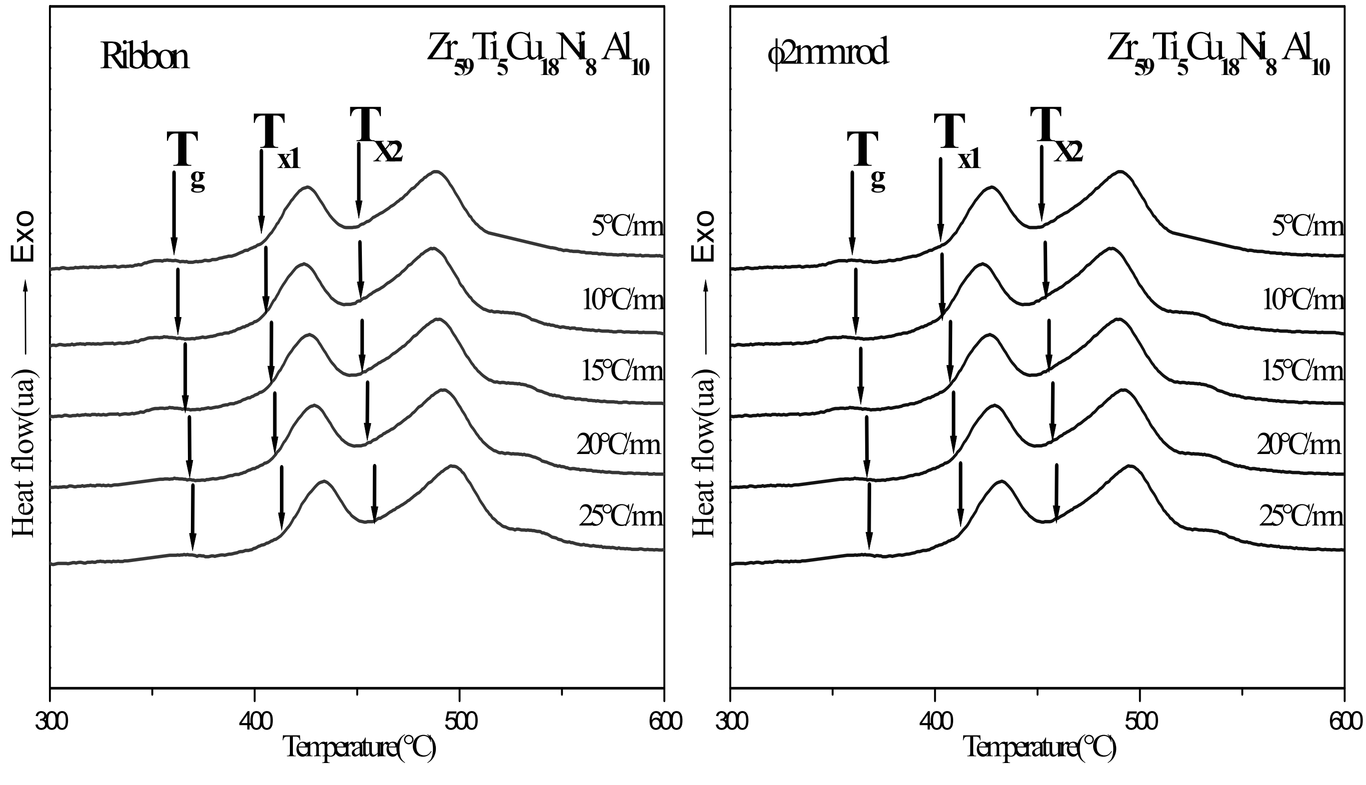


Fig. 1: DSC curves of $Zr_{59}Ti_5Cu_{18}Ni_8Al_{10}$ alloy ribbon and rods with diameters of 2mm at different heating rates.

Fig. 2 shows XRD pattern of the cast $Zr_{59}Ti_5Cu_{18}Ni_8\ Al_{10}$ rod with a diameter of 2 mm, together with the XRD pattern of the melt-spun glassy alloy ribbon. Only a broad peak is seen around a diffraction angle of 39° for the bulk sample and ribbon, indicating the formation of a glassy phase.

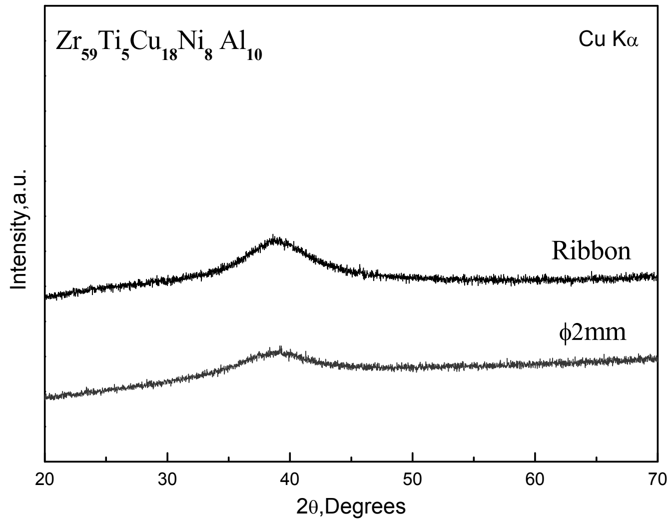


Fig. 2: XRD pattern of the cast $Zr_{59}Ti_5Cu_{18}Ni_8\ Al_{10}$ rod with a diameter of 2 mm, together with the XRD pattern of the melt-spun glassy alloy ribbon.

The critical cooling rate for glass formation, *R*c, is an important characteristic parameter for predicting the ease or difficulty of glass formability. It is defined as the minimum cooling rate necessary to keep the melt amorphous without detectable crystallization upon solidification. A slower *R*c indicates a greater glass-forming ability of an alloy system.

The room temperature compression results are in good agreement with the report. In addition, $Zr_{59}Nb_5\ Cu_{18}Ni_8\ Al_{10}$ alloy shows the compressive stress–strain curve at a strain rate of $5.10^{-4}\ s^{-1}$ (Fig.3). The fracture of the samples occurs at a fracture stress $\sigma_f$ of 1860 MPa and elastic a deformation up to a strain of about 1.9%.

The Young's modulus is determined as 97 GPa for the 2 mm diameter sample, which is larger than those of the $Zr_{65}A_{l7.5}Ni_{10}Cu_{17.5-x}Ag_x$ (x=5 and 10 at.%) BMGs, but is comparable to that of the annealed $Zr_{65}A_{l7.5}Ni_{10}Cu_{12.5}Ag_5$ alloy containing approximately 85% nanometer scaled I-phases and $Zr_{58}Al_9Ni_9Cu_{14}Nb_{10}$ alloy containing 90% quasicrystal. The elasticity is several times superior than that of $Al_{63.5}Cu_{24.5}Fe_{12}$ and $Al_{70}Pd_{20}Mn_{10}$ poly-crystalline icosahedral quasicrystals [12, 13], while the measured Young's modulus value is much lower than those of the conventional quasicrystals as shown in Table 2.

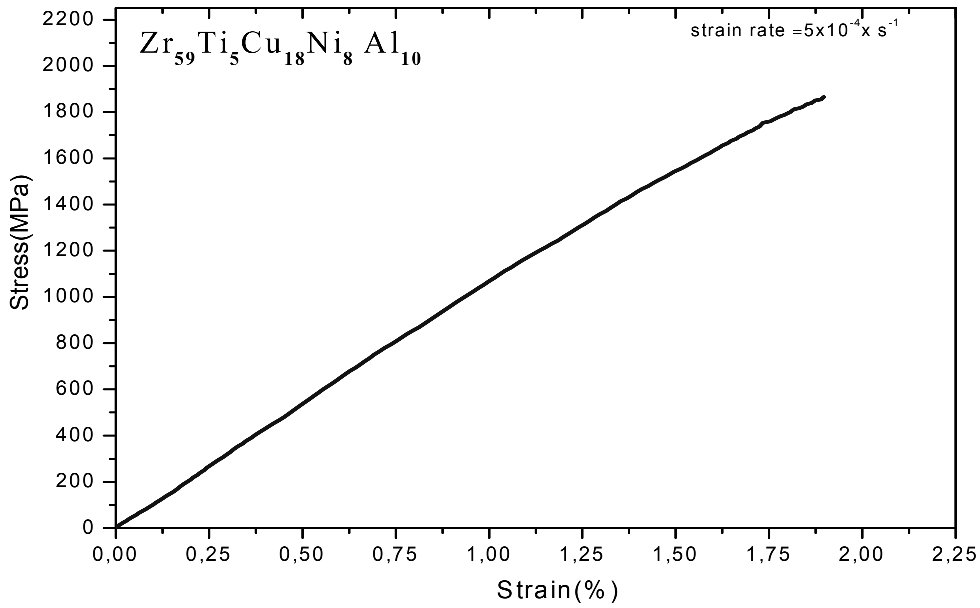


Fig. 3: Compressive stress–strain curves of cast Zr59Ti5Cu18Ni8 $Al_{10}$ glassy alloy rods under an niaxial compression testing at room temperature

Table 2: Mechanical properties of the present materials compared with Al- and Zr-based non-crystalline alloys.

| Materials | Phase constituents | Elastic stress limit $\sigma_f$ (Mpa) | Elastic deformation limit $\varepsilon_e$ (%) | Young's modulus E (GPa) |
|---|---|---|---|---|
| $Al_{70}Pd_{20}Mn_{10}$ [14] | I-phase | 520 (fracture) | 0.3 | 200 |
| $Al_{63}Cu_{25}Fe_{12}$ [15] | I-phase | 250 (fracture) | 0.35 | 172 [16] |
| $Zr_{65}Al_{7.5}Ni_{10}Cu_{12.5}Ag_5$ [17] | BMGs | 1650 (fracture) | 1.95 | 84.5 |
| $Zr_{65}Al_{7.5}Ni_{10}Cu_{12.5}Ag_5$ [17] | 85% quasicrystal +15% glass | 1200 (fracture) | 1.5 | 90 |
| $Zr_{58}Al_9Ni_9Cu_{14}Nb_{10}$ [18] | 90% quasicrystal +10% glass | 1800 (fracture) | 2.0 | 92 |
| $Zr_{59}Ti_5Cu_{18}Ni_8Al_{10}$ (this work) | BMGs | 1860(fracture) | 1.9 | 97 |

The fracture surfaces of $Zr_{59}Ti_5Cu_{18}Ni_8Al_{10}$ present an inhomogeneous deformation and fracture behaviour. For 2 mm-diameter cylinders, similar remelting features were observed on the fracture surface (Fig 4(a)).Most of the area of the fracture surface exhibits brittle features with rough rock-layer patterns (Fig. 4(b)). The rock-layers and deformation bands are main features on the fracture surface for alloy $Zr_{59}Ti_5Cu_{18}Ni_8Al_{10}$. The deformation bands with high protuberance reveal the large localized deformation before fracture. The remelting occurs on the fracture surface indicating large elastic strain energy and high local increase in temperature. This behavior is similar to that in single-phase BMGs, which can be qualitatively estimated by the following equation [19]:

$$\Delta T = V/V_f \times 1/C_p \times \sigma_f \varepsilon_e \qquad (1)$$

V and $V_f$ are samples volume and localized deformation volume, respectively. Cp is the specific heat capacity, $\sigma_f$ is the fracture strength and $\varepsilon_e$ is the elastic strain. This equation is derived by correlating the total elastic strain energy with the temperature increase in the localized deformation region in the fracture surface. $\Delta T$ is proportional to $\sigma_f$ and $\varepsilon_e$, and inversely proportional to $V_f$, which means that high strength, low Young's modulus and highly localized deformation region can give a large increase in temperature on the local fracture surface. If the melting temperature is low, some remelting phenomena can be observed on the fracture surface. The present $Zr_{59}Ti_5Cu_{18}Ni_8Al_{10}$ alloy satisfy these conditions, thus the remelting behavior occurs during fracture.

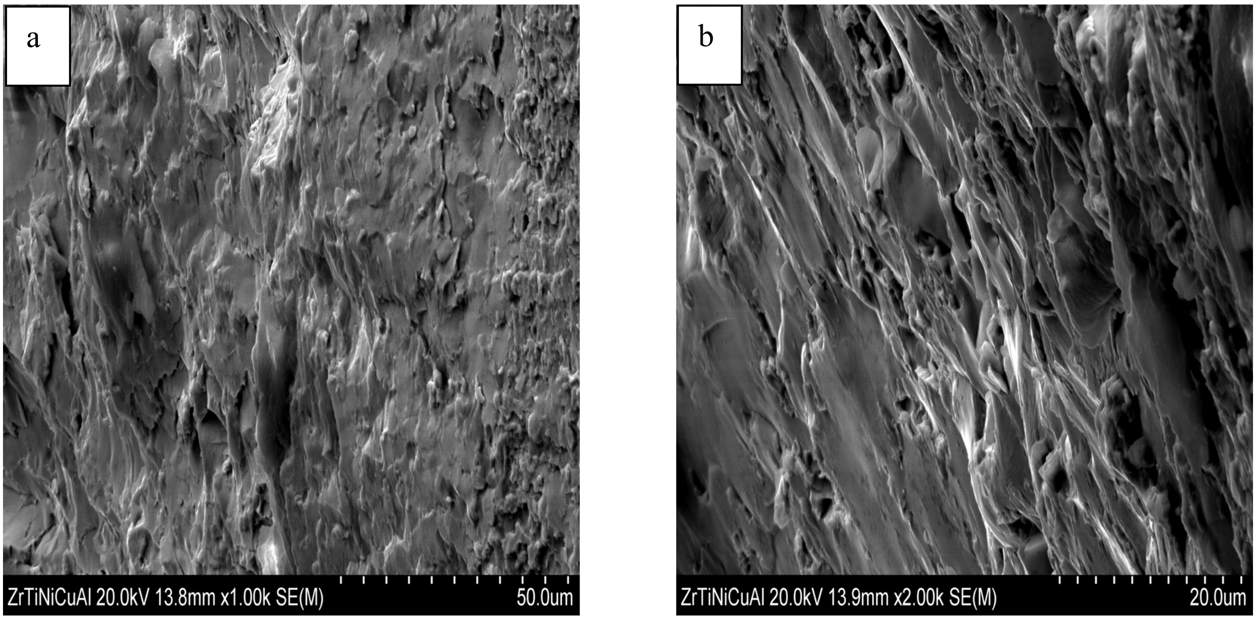


Fig. 4: SEM of the fracture surfaces of $Zr_{59}Ti_5Cu_{18}Ni_8\,Al_{10}$ amorphous rod in as –cast state with diameter of 2 mm. (a) Shows the brittle fracture surface and local remelting,(b) The rock layer features.

Fig. 5 shows some Vickers indentations obtained for different indentation loads. The profiles of indentation trace were analyzed by optical microscopy. The results obtained for the stem of $Zr_{59}Ti_5Cu_{18}Ni_8\,Al_{10}$ with 2 mms in diameter load of 300g HV 516, in addition hardness stripped HV 505 with a load of 1000g, with the last load of 3000g hardness is HV 496.For the three loads applied one a does not observe any cracks when can about it noted around the impressions.

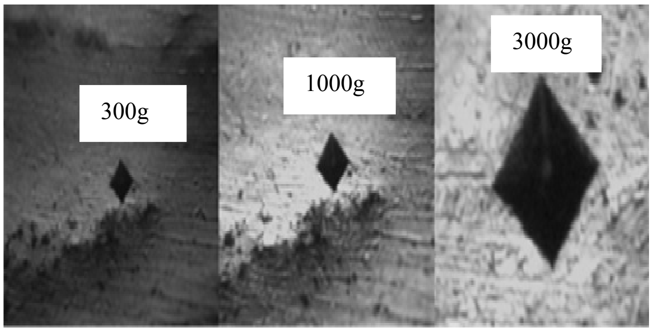


Fig. 5: Optical morphologies of the Vickers' indentations on the as-cast $Zr_{59}Ti_5Cu_{18}Ni_8\,Al_{10}$ alloy under the loads ranging from 300 g, 1000g and 3000 g.

The results of chemical analysis of the $Zr_{59}Ta_5Cu_{18}Ni_8\,Al_{10}$ rod with a diameter 2 mm by EDS attached to SEM was show on Fig. 6.

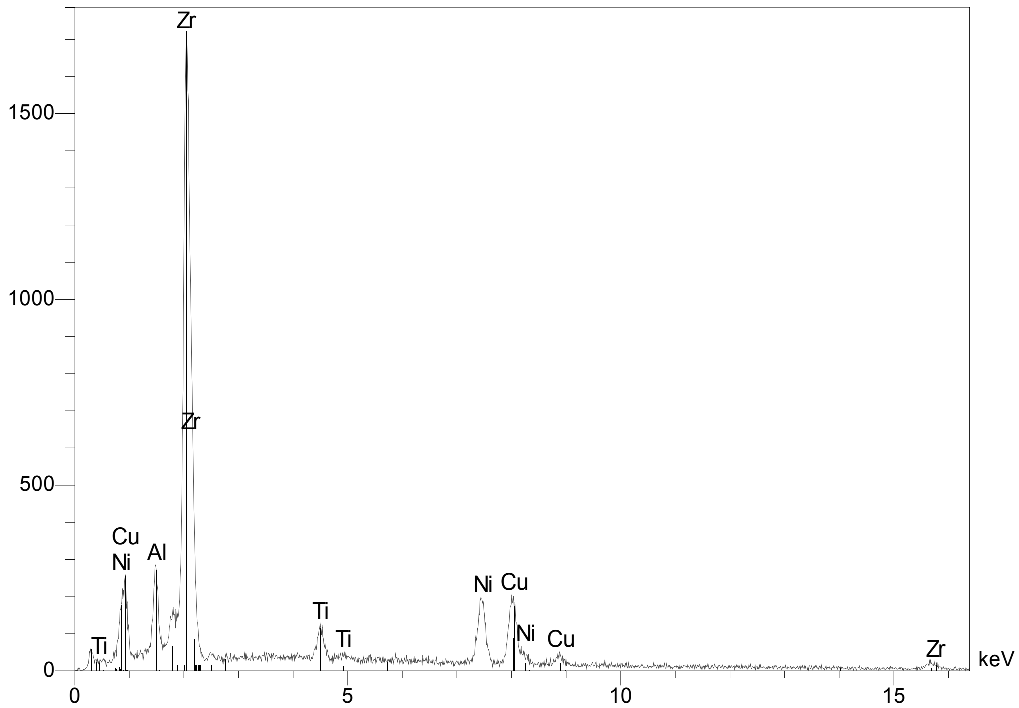


Fig. 6: Energy dispersive spectra of the $Zr_{59}Ti_5Cu_{18}Ni_8\,Al_{10}$ alloy.

The structural evolution during heating was investigated by XRD. The diffraction patterns of rod form with diameter of 2 mm at prepared through water-cooled copper mold casting heated to different temperatures are shown in Fig. 7, together with the pattern of the as-prepared sample. the cast rod of Φ2 mm exhibit the typical broad maxima characteristic for amorphous materials and no trace of crystalline phases, indicating that they are in the amorphous state. The phase formation reflect at the beginning (T=400°C) and at the second (T=450°C) of the single exothermic event. Obviously, the first step of devitrification is mostly linked with the formation of quasicrystalline phase, as other crystalline phase (cubic $NiZr_2$, tetragonal $CuZr_2$, hexagonal $Al_3Zr_4$ and unidentified phase(s)) only exist in a low volume fraction at that temperature. Further heating to the second of the transformation step leads to significant growth of the crystalline phases (e.g. tetragonal $NiZr_2$), whereas the metastable quasicrystalline phase completely disappears.

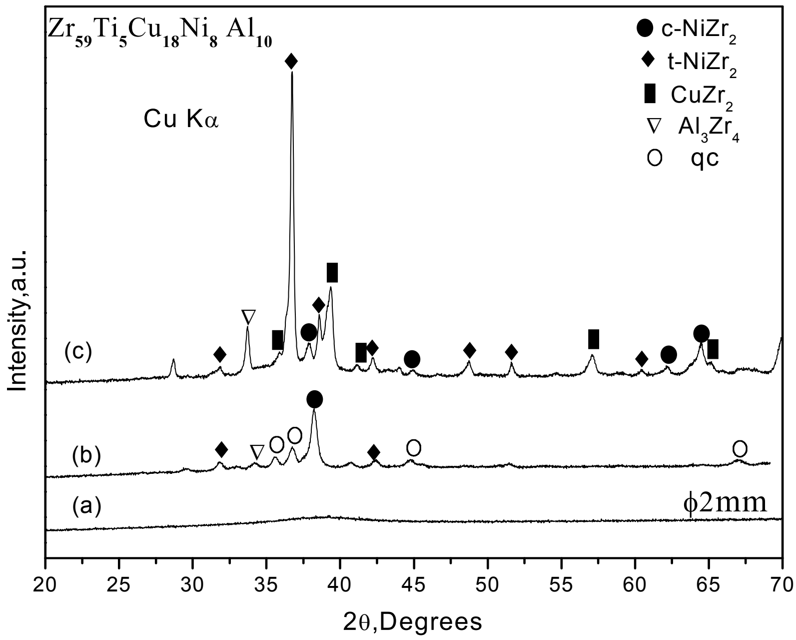


Fig. 7: X-ray diffraction patterns for as-cast amorphous specimen (a) specimens aged at 400 °C (b) and 450°C (c) for 9 min.

## 4. Conclusion

In conclusion, The comparison between the ribbon were obtained directly from the melt-spinning technique and the same alloy produced by injection casting of the molten alloy into copper molds with cylindrical cavities reveals that both types of samples are characterized by the formation phase amorphous obtained in X-ray diffraction .
The bulk glassy rods possess good mechanical properties, the compressive fracture strength and elastic strain to fracture of the amorphous alloy with 2, 13 at. % also exhibit ultrahigh fracture strength of 1860 MPa, Young's modulus of 97 GPa.
The stable crystalline phases include cubic $NiZr_2$, tetragonal $CuZr_2$, hexagonal $Al_3Zr_4$ and e.g. tetragonal $NiZr_2$ after complete crystallization of the as-cast 2 mm aged at 450°C for 9 min.

## Acknowledgement

The authors are grateful to INRIM - Torino of the Univerity of Torino for providing experimental facilities.We thanks supports of Prof. M. Barrico for the synthesis of the samples and SEM pictures, XRD analysis.

## References

[1] Miracle D. B., Egami T., Flores K. M., Kelton K. F., MRS Bull, **32**(2007) 629
[2] Ashby M. F., Greer A. L., Scr Mater **54** (2006) 321
[3] Lin X. H., Johnson W. L., Rhim W.K., Mater Trans JIM, **38** (1997) 473
[4] Xing L.Q, Ochin P., J. Mater Sci Lett, **16** (1997) 1277
[5] Kündig A.A., Löffler J.F., Johnson W.L., Uggowitzer P.J., Thiyagarajan P., Scr Mater **44** (2001)1269
[6] Kühn U., Eymann K., Mattern N., Eckert J., Gebert A., Bartusch, B., *et al.,* Acta Mater, **54** (2006) 4685
[7] Scully J. R., Gebert A., Payer J. H., J. Mater. Res., **22 (2007)** 302
[8] Latanision R. M., Turn Jr. J. C., Compeau C. R., Proc Int Conf on Mechanical Behaviour of Materials [ICM 3]. Cambridge, England, August (20–24; 1979).
[9] Archer M. D., Corke C. C., Harji, B .H., Electrochim Acta, **32**(1987)13
[10] Hashimoto K., *Metastable alloys*. In: Winston Revie E, editor. Uhlig's Corrosion Handbook. 2nd ed. John Wiley & Sons, Inc., (2000) 929
[11] Scully, J. R., Lucente, A. *Corrosion of amorphous metals*. In: Cramer SD, Covino Jr B, editors. ASM Handbook, vol. 13B. Metals Park, OH: American Society for Metals (2005), 476
[12] Q. J. Chen, J. Shen, D. L. Zhang, H. B. Fan, J. F. Sun, J. Mater. Res. **22** (2007) 358
[13] F. F. Wu, Z. F. Zhang, B. L. Shen, S. X. Mao, J. Eckert, Adv. Eng. Mater. **10** (2008) 727
[14] Koster U, Liebertz H, Liu W. Mater Sci Eng **A 777**, (1994)181e182
[15] Vanderwal J. J, Zhao P., Walton D. Phys Rev **B46**, (1992) 501
[16] Inoue A., Zhang T., Chen M.W., Sakurai T., Mater Trans JIM **40**, (1999)1382
[17] J. B. Qiang, W. Zhang , Guoqiang Xie, Hisamichi Kimura, C. Dong, A. Inoue. Intermetallics **15** (2007) 1197e1201
[18] Z. F. Zhang, G. He, J. Eckert, L. Schultz, Phys. Rev. Lett. **91** (2003) 045505
[19] C. T. Liu, L. Heatherly, D. S. Eaton, C. A. Carmichael, J. H. Schneibel, C. H. Chen, J. L.,Wright, M. H. Yoo, J. A. Horton, A. Inoue, Metall. Mater. Trans. 29A (1998) 1811